Behavioral/Cognitive

Locus Coeruleus Integrity Is Linked to Response Inhibition Deficits in Parkinson's Disease and Progressive Supranuclear Palsy

Rong Ye,[1,2,3*] Frank H. Hezemans,[3,4,5*] Claire O'Callaghan,[6,7] Kamen A. Tsvetanov,[4,8] Catarina Rua,[3] P. Simon Jones,[3] Negin Holland,[3] Maura Malpetti,[3] Alexander G. Murley,[3] Roger A. Barker,[9,10] Caroline H. Williams-Gray,[9] Trevor W. Robbins,[8,11] Luca Passamonti,[3,12†] and James B. Rowe[3,4,11†]

[1]Research Center for Translational Medicine, The Second Affiliated Hospital of Anhui Medical University, Hefei, Anhui, 230032, China, [2]School of Mental Health and Psychological Sciences, Anhui Medical University, Hefei, Anhui, 230032, China, [3]Department of Clinical Neurosciences, Cambridge University Hospitals NHS Trust, University of Cambridge, Cambridge, CB2 0SZ, United Kingdom, [4]MRC Cognition and Brain Sciences Unit, University of Cambridge, Cambridge, CB2 7EF, United Kingdom, [5]Donders Institute for Brain, Cognition and Behaviour, Radboud University, 6525 GD Nijmegen, The Netherlands, [6]Department of Psychiatry, University of Cambridge, Cambridge, CB2 0SZ, United Kingdom, [7]Brain and Mind Centre and School of Medical Sciences, Faculty of Medicine and Health, University of Sydney, Sydney 2050, New South Wales, Australia, [8]Department of Psychology, University of Cambridge, Cambridge, CB2 3EA, United Kingdom, [9]John van Geest Centre for Brain Repair, Department of Clinical Neurosciences, University of Cambridge, Cambridge, CB2 0SZ, United Kingdom, [10]Wellcome-MRC Stem Cell Institute, University of Cambridge, Cambridge, CB2 0AW, United Kingdom, [11]Behavioural and Clinical Neuroscience Institute, University of Cambridge, Cambridge, CB2 3EA, United Kingdom, and [12]Institute of Molecular Bioimaging and Physiology, National Research Council, 88100, Catanzaro, Italy

Parkinson's disease (PD) and progressive supranuclear palsy (PSP) both impair response inhibition, exacerbating impulsivity. Inhibitory control deficits vary across individuals and are linked with worse prognosis, and lack improvement on dopaminergic therapy. Motor and cognitive control are associated with noradrenergic innervation of the cortex, arising from the locus coeruleus (LC) noradrenergic system. Here we test the hypothesis that structural variation of the LC explains response inhibition deficits in PSP and PD. Twenty-four people with idiopathic PD, 14 with PSP-Richardson's syndrome, and 24 age- and sex-matched controls undertook a stop-signal task and ultrahigh field 7T magnetization-transfer-weighted imaging of the LC. Parameters of "race models" of go- versus stop-decisions were estimated using hierarchical Bayesian methods to quantify the cognitive processes of response inhibition. We tested the multivariate relationship between LC integrity and model parameters using partial least squares. Both disorders impaired response inhibition at the group level. PSP caused a distinct pattern of abnormalities in inhibitory control with a paradoxically reduced threshold for go responses, but longer nondecision times, and more lapses of attention. The variation in response inhibition correlated with the variability of LC integrity across participants in both clinical groups. Structural imaging of the LC, coupled with behavioral modeling in parkinsonian disorders, confirms that LC integrity is associated with response inhibition and LC degeneration contributes to neurobehavioral changes. The noradrenergic system is therefore a promising target to treat impulsivity in these conditions. The optimization of noradrenergic treatment is likely to benefit from stratification according to LC integrity.

Key words: **7T-MRI; cognitive modeling; locus coeruleus; Parkinson's disease; progressive supranuclear palsy; response inhibition**

Received Jan. 19, 2022; revised June 21, 2023; accepted June 22, 2023.

Author contributions: R.Y., F.H.H., C.O., K.A.T., R.A.B., C.H.W.-G., T.W.R., L.P., and J.B.R. designed research; R.Y., F.H.H., C.O., C.R., N.H., M.M., A.G.M., R.A.B., and C.H.W.-G. performed research; R.Y., F.H.H., C.O., K.A.T., C.R., P.S.J., M.M., and A.G.M. analyzed data; R.Y., F.H.H., L.P., and J.B.R. wrote the first draft of the paper; R.Y., F.H.H., C.O., K.A.T., C.R., P.S.J., N.H., M.M., A.G.M., R.A.B., C.H.W.-G., T.W.R., L.P., and J.B.R. edited the paper; R.Y., F.H.H., C.O., K.A.T., L.P., and J.B.R. wrote the paper; K.A.T. contributed unpublished reagents/analytic tools.

This work was supported by Parkinson's United Kingdom K-1702; the Cambridge Center for Parkinson-Plus; the China Scholarship Council; Australian National Health and Medical Research Council Neil Hamilton Fairley Fellowship GNT1091310; Cambridge Trust Vice-Chancellor's Award and Fitzwilliam College Scholarship; the Association of British Neurologists, Patrick Berthoud Charitable Trust RG99368; Medical Research Council SUAG/051 G101400; MR/P01271X/1; James S. McDonnell Foundation 21st Century Science Initiative Scholar Award in Understanding Human Cognition; Medical Research Council RCUK/UKRI Research Innovation Fellowship MR/R007446/1; and National Institute for Health Research Cambridge Clinical Research Facility and the National Institute for Health Research Cambridge Biomedical Research Center BRC-1215-20014 and NIHR203312. The views expressed are those of the authors and not necessarily those of the National Health Service, the National Institute for Health Research or the Department of Health and Social Care. For the purpose of open access, the author has applied a CC BY public copyright license to any Author Accepted Manuscript version arising from this submission.

*R.Y. and F.H.H. contributed equally to this work as first authors.

†L.P. and J.B.R. contributed equally to this work as senior authors.

The authors declare no competing financial interests.

Correspondence should be addressed to Rong Ye at ronye.uk@gmail.com.

https://doi.org/10.1523/JNEUROSCI.0289-22.2023

Significance Statement

Response inhibition deficits contribute to clinical symptoms and poor outcomes in people with Parkinson's disease and progressive supranuclear palsy. We used cognitive modeling of performance of a response inhibition task to identify disease-specific mechanisms of abnormal inhibitory control. Response inhibition in both patient groups was associated with the integrity of the noradrenergic locus coeruleus, which we measured *in vivo* using ultra-high field MRI. We propose that the imaging biomarker of locus coeruleus integrity provides a trans-diagnostic tool to explain individual differences in response inhibition ability beyond the classic nosological borders and diagnostic criteria. Our data suggest a potential new stratified treatment approach for Parkinson's disease and progressive supranuclear palsy.

Introduction

Progressive supranuclear palsy (PSP) and Parkinson's disease (PD) have distinct neuropathology and clinical features (Hauw et al., 1994; Braak et al., 2003), but both can cause an impairment of response inhibition that contributes to disinhibited behavior and impulsivity, which is associated with poor clinical outcomes (Ryu et al., 2019; Erga et al., 2020; Murley et al., 2021). Impulsivity is a multifaceted behavioral construct, including abnormal sensitivity to reward, intolerance to delayed reward and a failure to inhibit inappropriate responses (Dalley et al., 2011; Dalley and Robbins, 2017). Here we focus on response inhibition, as the execution of responses represents a point of convergence for upstream changes in cognition and behavioral decisions in impulsivity.

Noradrenergic manipulations influence response inhibition, especially the cancellation of a response, in preclinical models (Robinson et al., 2008; Bari et al., 2011), healthy humans (Chamberlain et al., 2009), attention deficit disorders (Chamberlain et al., 2007; Del Campo et al., 2011), and PD (Averbeck et al., 2014; Kehagia et al., 2014; Z. Ye et al., 2015; Borchert et al., 2016). In PSP and PD, the locus coeruleus (LC) is an early site of pathologies (Cash et al., 1987; Zweig et al., 1993; Li et al., 2019; Kaalund et al., 2020) whose structural integrity is associated with behavioral performance and neural substrate of response inhibition (Tomassini et al., 2022; R. Ye et al., 2022). The LC-noradrenergic system is therefore a promising route to ameliorate response inhibition deficits in diverse neurologic and psychiatric disorders.

The heterogeneity in LC damage has been linked to variability in the response to drugs that increase noradrenergic transmission, such as atomoxetine (O'Callaghan et al., 2021). To facilitate more targeted treatment of impulsivity in PSP and PD, it is necessary to quantify LC structural integrity *in vivo* and determine its relationship to response inhibition. Specialist MRI sequences for ultrahigh field scanners (7T) have enabled sensitive and well-tolerated quantification of LC pathology (Wang et al., 2018; Betts et al., 2019b; O'Callaghan et al., 2021; R. Ye et al., 2022). The contrast and the resolution ($400 \times 400 \times 500$ μm) provided by the specialist sequence and the 7T MR scanner are sufficient to examine regional effects of pathology within the LC (Mason and Fibiger, 1979; Loughlin et al., 1986), and an advantage over the contrast and resolution at 3T.

The LC degeneration and noradrenergic deficits may influence response inhibition at both motor and cognitive (decisional) levels, given the widespread cortical LC projections (Sara, 2009). Response inhibition can be measured using performance on a stop signal task, but singular parameters of performance may obscure the complexity of underlying decision mechanisms. A multivariate model of computational parameters of response inhibition overcomes this limitation, to distinguish motor, attentional, and decisional components of inhibition (Zhang et al., 2016; Murley et al., 2020; O'Callaghan et al., 2021).

In this study, we performed parametric analyses of the processes underlying the stop signal task, estimated with hierarchical Bayesian models, to advance our understanding of the response inhibition deficits in PD and PSP. These models explain response accuracy and reaction times (RTs) as function of a race between three processes: a stop process, a go process for the response that matches the choice stimulus, and a go process for the response that mismatches the choice stimulus (Logan et al., 1984; Matzke et al., 2019, 2020). The models also estimate attentional failures to trigger the stop and go processes. The go processes were parameterized as sequential sampling models, in which evidence accumulates stochastically until a response threshold is reached. The mean finish time of the stop process served as the estimate of the stop signal RT (SSRT).

We tested the hypothesis that these parameters of response inhibition relate to LC structural integrity at an individual participant level, as measured *in vivo* using 7T-MRI. We predicted that the response inhibition deficits characterizing PSP and PD would be associated with reduced LC integrity. We investigated the multivariate relationship between LC integrity and response inhibition because of the multivariate nature of the model parameters and the topographic organization of the LC, identifying where its modulation is exerted by subpopulations of LC neurons (Chandler et al., 2019) projecting to different brain regions (Loughlin et al., 1986).

Materials and Methods

Participants

Fourteen patients with probable PSP-Richardson's syndrome (MDS 2017 criteria), 24 with idiopathic PD (UK Parkinson's disease Brain Bank criteria), and 24 age- and sex-matched healthy controls were included in the study (as in R. Ye et al., 2022). Controls did not use psychoactive medications, and exclusions criteria for all participants included history of stroke, severe medical comorbidity, and any contraindications to 7T-MRI. None of the patients met criteria for impulse control disorders, based on clinical impression and/or the Questionnaire for Impulsive-Compulsive Disorders. Participants were not demented, based on a Mini-Mental State Examination score >26 and clinical impression. All patients with PD and 10 of 14 PSP patients were on dopaminergic medications (Table 1). The study was approved by the local Cambridge Research Ethics Committees. Participants provided written informed consent according to the Declaration of Helsinki.

Experimental design

All participants underwent a structured clinical, cognitive, and behavioral assessment (Table 1). The LC integrity was measured *in vivo* in a 7T-MRI scan on the same study session. Response inhibition was measured using a stop-signal paradigm. All participants completed the stop-signal task on the same testing session of the MRI scan and task battery, except for 18 patients with PD who were part of a single-dose, placebo-

Table 1. Demographics (mean and SD) of participants and clinical assessments[a]

	Descriptive			*p* values for pairwise tests		
	HC	PD	PSP	HC vs PD	HC vs PSP	PD vs PSP
Age (yr)	65.5 (5.5)	67.2 (7.4)	69.7 (7.7)	0.66	0.164	0.52
Education (yr)	14.8 (3.1)	14 (2.3)	12.3 (2.8)	0.584	0.021	0.15
Male/female	13/11	18/6	8/6	0.131	0.859	0.253
MMSE	29.75 (0.53)	29.52 (0.65)	28.5 (1.74)	0.649	<0.001[b]	0.009
MoCA	28.58 (1.44)	27.88 (1.87)	24 (3.94)	0.557	<0.001[b]	<0.001[b]
ACER-total	97.71 (3.25)	95.25 (3.6)	87.21 (7.17)	0.153	<0.001[b]	<0.001[b]
Apathy Scale	10.38 (5.25)	12.42 (5.55)	20 (9.49)	0.528	<0.001[b]	0.003
BIS	55.71 (9.56)	58.69 (10.21)	63.86 (12.44)	0.591	0.063	0.316
HADS-Depression	2.83 (2.84)	4.25 (2.79)	7.43 (4.27)	0.281	<0.001[b]	0.012
HADS-Anxiety	4.29 (3.53)	5.17 (3.16)	6.57 (3.2)	0.634	0.111	0.424
RBDSQ	—	5.38 (3.69)	3.07 (1.82)	—	—	0.036
Disease duration (yr)	—	5.09 (3.05)	4.24 (2.68)	—	—	0.397
LEDD	—	646.6 (509.53)	323.57 (389.4)	—	—	0.038
UPDRS-III	—	28.21 (12.21)	33.07 (6.96)	—	—	0.182
PSPRS	—	—	30.79 (9.11)	—	—	—

[a]Group difference in sex was examined using χ^2 test. A one-way ANOVA was used for group difference with *post hoc* Tukey HSD *p* values provided for pairwise comparisons. RBDSQ, disease duration and UPDRS-III were compared with independent-samples *t* test between PD and PSP. MMSE, Mini-Mental State Examination; MoCA, Montreal Cognition Assessment; ACER, Addenbrooke's Cognitive Examination Revised; BIS, Barratt Impulsiveness Scale; HADS, Hamilton Anxiety and Depression Scale; RBDSQ, REM Sleep Behaviors Screening Questionnaire; LEDD, Levodopa equivalent daily dose; UPDRS, Unified Parkinson's Disease Rating Scale; PSPRS, PSP Rating Scale.
[b]Significant *p* values ($p < 0.0016$, equivalent to $p < 0.05$ with Bonferroni correction).

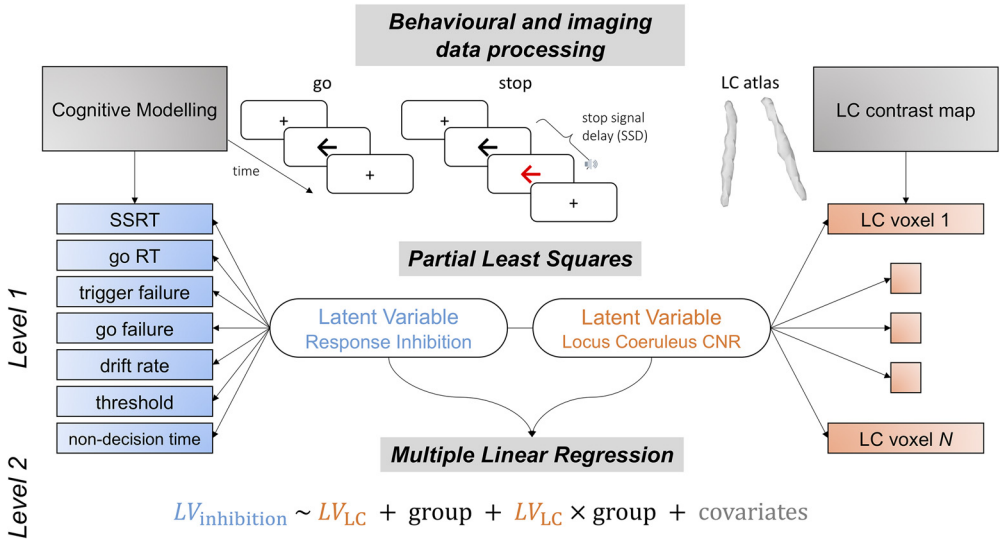

Figure 1. Schematic representation of data analysis pipeline. The trial-by-trial stop signal task performance was subjected to a two parametric race model following ex-Gaussian and shifted Wald distributions. An array of behavioral parameters were estimated hierarchically from the models for both stop and go response, including SSRT, go RT, trigger failure, go failure, drift rate (ν), response threshold (B), and nondecision time (t_0). These parameters altogether provided more mechanistic understanding of response inhibition. The LC integrity was assessed by computing voxel-wise CNR and extracted using an independent LC probability atlas. The multivariate relationship between LC integrity and response inhibition was then examined using PLS on resulting behavioral and imaging matrices from previous data processing steps. Significant pairs of latent variables were identified with the permutation test. The contribution of LC in response inhibition was finally confirmed in linear regression models with individual subject loading scores on the inhibition latent variable as dependent variable, loading scores on the LC latent variable, group and nuisance covariates as predictors.

controlled, crossover drug study where the relationship between LC integrity and drug responsiveness was investigated (O'Callaghan et al., 2021). The behavioral performance of these patients was examined for the placebo session, and potential placebo or practice effects were explicitly modeled (see Statistical analysis).

Stop-signal task

For a detailed description of the stop signal task design, we refer the reader to Murley et al. (2020) or O'Callaghan et al. (2021), who used an identical paradigm. In brief, the stop-signal task involves a two-choice RT "go" task, which was occasionally interrupted by a "stop signal." For the go task, participants were instructed to indicate the direction of a black arrow presented at the center of the screen by pressing a left or right button. On stop trials, the arrow changed to a red color in conjunction with a tone (i.e., the stop signal), and participants were instructed to withhold their initiated response (Fig. 1, top left). The stop signal occurred after a variable delay (i.e., the stop-signal delay), the length of which was determined by an adaptive staircase method. The stop-signal delay ranged from 50 to 1500 ms and increased or decreased by 50 ms after a successful or failed stop trial, respectively.

Modeling of response inhibition

Parametric race models. We applied two complementary race models to the stop-signal task data. The first model assumed that the finish time distributions of the stop and go processes followed ex-Gaussian distributions (Heathcote et al., 1991), with mean (μ) and SD (σ) of the Gaussian component, and mean τ of the exponential component. The mean finish time of each process was estimated as the mean of the corresponding ex-Gaussian distribution, which is given by $\mu + \tau$. The mean finish times

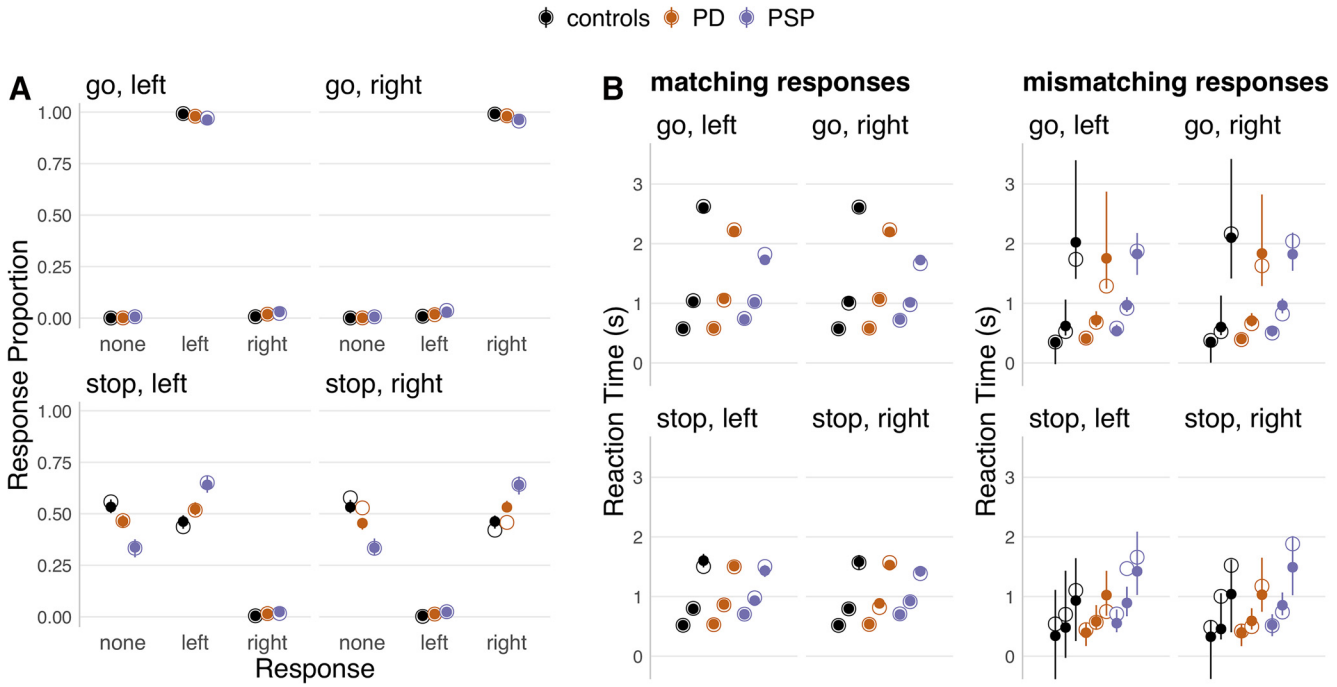

Figure 2. Posterior predictive checks of response proportions and RTs. For each panel, the observed data (hollow dots) are compared with data from 100 simulated participants, drawn randomly from the posterior predictive distribution of the final model fit (solid dots and error bars). Each panel represents one unique combination of trial type (go vs stop) and choice stimulus (left vs right). The results are plotted separately for each group (controls, PD, PSP). For response proportions (***A***), the results are additionally plotted separately for each response option along the *x* axis (no response, left, right). For RTs (***B***), the 10th, 50th, and 90th percentiles of the RT distributions (bottom, middle, top dot) are plotted separately for response accuracy (matching vs mismatching), since mismatching responses constituted a very small proportion of the data. For each panel, the dots represent group-level medians, and the error bars indicate the group-level 95% QIs of the simulated data.

of the stop process and matching go process were taken as the SSRT and go RT, respectively.

The second model was similar, except that the finish time distributions of the go processes were assumed to follow shifted Wald distributions (Matzke et al., 2020). The Wald distribution describes the first-passage time distribution of a single-boundary diffusion process, where evidence accumulates stochastically at a positive mean rate ν (compare the drift rate) until a threshold B is reached. A subject-specific constant nondecision time t_0 shifts the lower bound of the distribution to account for peripheral processes, such as stimulus encoding and motor output. The shifted Wald distribution therefore enables a process model that explains how the go RT distributions were generated.

Both models additionally included the probabilities of attentional failures related to the stop process (trigger failure) and go processes (go failure). Thus, the first model featured 11 free parameters: three ex-Gaussian parameters for each of the three processes, and the trigger and go failure probabilities. The second model featured nine free parameters: separate drift rates for the matching and mismatching go processes, a threshold and nondecision time that were shared across the go processes, three ex-Gaussian parameters for the stop process, and the trigger and go failure probabilities.

Hierarchical Bayesian modeling was used to fit each model to the observed task data, separately for the PSP, PD, and control groups. Markov Chain Monte Carlo (MCMC) sampling methods were used to estimate the posterior distributions of all group- and participant-level parameters. We assigned broad ("weakly informative") priors on the group-level means and SDs of the model parameters, to regularize the inference and prevent parameters from taking on extreme values. These priors were based on suggested settings from the model developers (Heathcote et al., 2019), with slight adjustments to account for slower response times in older age and neurodegenerative disease. Specifically, for the ex-Gaussian model, the prior on the group-level mean of the μ parameter was N_+ (1.5, 1) for the go processes and N_+ (1, 1) for the stop process; the prior on the group-level means of the σ and τ parameters was N_+ (0.2, 1); and the prior on the group-level means of the probit-transformed attentional failure probabilities was $N\,(\phi^{-1}(0.1, 1)$. Here, N (μ, σ) denotes a normal distribution with mean and SD; $N_+(\mu, \sigma)$ denotes a normal distribution truncated to only allow positive values; and $\phi^{-1}(p)$ denotes the probit function (i.e., the inverse cumulative distribution function of the standard normal distribution) evaluated at probability p. For the hybrid Wald/ex-Gaussian model, the prior on the group-level mean of the drift rate ν was N_+ (2, 3) for the matching go process and N_+ (1, 3) for the mismatching go process; the prior on the group-level mean of the threshold B was N_+ (2, 1); and the prior on the group-level mean of the nondecision time t_0 was N_+ $(0.1, \infty)(0.3, 0.25)$, where $N_{(a,b)}(\mu, \sigma)$ denotes a normal distribution with lower truncation a and upper truncation b. The priors on the group-level means of the parameters of the stop runner and the probit-transformed attentional failure parameters were the same as in the ex-Gaussian model. For all parameters in both the ex-Gaussian model and the hybrid Wald/ex-Gaussian model, the prior on the group-level SD was an exponential distribution with a rate of 1.

Sampling convergence was confirmed by visual inspection of the time series plots of the MCMC samples, and by the potential scale reduction statistic R-hat (<1.1 for all parameters). The absolute goodness of fit was assessed by visually comparing the observed data to simulated data generated from the model's posterior predictive distribution (Fig. 2).

Model fitting was performed using the Dynamic Models of Choice toolbox (Heathcote et al., 2019) implemented in R (version 3.6.1). The number of sampling chains was set to 3 times the number of free parameters. Automated procedures were used to continue sampling until convergence was reached (h.run.unstuck.dmc and h.run.converge.dmc functions in the Dynamic Models of Choice toolbox). After this, an additional 500 iterations were obtained for each chain to create a final posterior distribution for each parameter, which was used for statistical analyses.

MRI acquisition and processing

Participants were scanned on a 7T Magnetom Terra (Siemens) with a 32-channel receive head coil (Nova Medical). Following the acquisition

and processing protocol described previously (O'Callaghan et al., 2021; R. Ye et al., 2021, 2022), the LC was imaged using a near-isotropic 3D magnetization transfer (MT) weighted sequence at submillimeter resolution (112 oblique, axial slices oriented perpendicular to the long axis of the brainstem). The sequence applied a train of 20 Gaussian-shape RF pulses at 6.72 ppm off-resonance, 420° flip angle, followed by a turbo-flash readout (TE = 4.08 ms, TR = 1251 ms, flip angle = 8°, voxel size = 0.4 × 0.4 × 0.5 mm^3, 6/8 phase and slice partial Fourier, bandwidth = 140 Hz/px, no acceleration, 14.3% oversampling, TA ~ 7 min). For each subject, the transmit voltage was adjusted based on the average flip angle in the central area of the pons obtained from a B1 precalibration scan. Two images with MT presaturation pulses were acquired, then averaged offline to enhance signal-to-noise ratio. One image without MT effect (MT-off) was additionally obtained for registration. A high-resolution T1-weighted structural image (0.7 mm isotropic) was acquired using an MP2RAGE sequence with the UK7T Network harmonized protocol (Clarke et al., 2020): TE = 2.58 ms, TR = 3500 ms, BW = 300 Hz/px, voxel size = 0.7 × 0.7 × 0.7 mm^3, FOV = 224 × 224 × 157 mm^3, acceleration factor (A ≫ P) = 3, flip angles = 5/2°. MT and T1 images were preprocessed using the Advanced Normalization Tools (ANTs version 2.2.0). MT images were N4-bias field-corrected, then coregistered to the isotropic 0.5 mm ICBM152 (International Consortium for Brain Mapping) T1-weighted asymmetric nonlinear template (Fonov et al., 2011) following a T1-driven coregistration approach. The individual registration roadmap was initiated from the estimation between averaged MT image and the MT-off image (rigid only), then moved to the coregistration between MT and T1 modality in the following order: MT-off to MT (rigid only), individual T1 to MT-off (rigid only), individual T1 to T1 group template (rigid, Affine and SyN), and finally T1 group template to the ICBM152 template (rigid, Affine and SyN). The detailed parameter settings used for coregistration and T1 template construction can be downloaded from the NITRC webpage of our 7T LC atlas for the replication of our image processing procedures (https://www.nitrc.org/projects/lc_7t_prob/).

The coregistered MT images were converted to contrast-to-noise (CNR) maps by subtracting the mean and dividing by the SD of the signal in a central pontine reference region (O'Callaghan et al., 2021; R. Ye et al., 2022). This cubic pontine reference region (4 × 4 × 4.5 mm^3) was chosen as a measurement source of noise because of its proximity to the LC. A probabilistic LC atlas was applied on the CNR maps with a conservative threshold (25%) to extract voxel-wise LC CNRs for later statistical tests and slice-wise means for group comparisons. The calculation of CNR maps was implemented using *fslmaths* function, and *fslstats* was used for the extraction of CNRs within the probabilistic LC atlas. Structural T1-weighted images were subjected to FreeSurfer (version 6.0) *recon-all* pipeline with *-highres* and *-brainstem* options. The resulting total intracranial and brainstem subregion volumes were used for the estimation of global and local atrophy, respectively. Signal quality was measured with signal-to-noise ratio (SNR) by calculating the division between the mean and the SD of the raw signal on coregistered MT images for subregions and the whole LC. Potential group differences and correlations with LC integrity measures of brainstem volumes and regional SNRs were tested using ANOVAs and linear regression models, respectively.

Statistical analysis

Group differences in response inhibition parameters. We analyzed group differences in mechanisms of response inhibition by examining the posterior distributions of the group-level means of the race model parameters. For each posterior distribution, we took the median as the posterior estimate, and the 95% quantile interval (QI) as the range of plausible values. We derived posterior distributions for group contrasts by subtracting the set of MCMC samples of the two groups under consideration. For each group contrast, we computed the probability of direction (P_{dir}) as an index of the presence of an effect (Makowski et al., 2019). This measure indicates the proportion of the contrast's posterior distribution that is strictly positive or negative (whichever is the most probable). P_{dir} can be directly interpreted as the probability that a group difference is non-zero, and is therefore not subject to a particular significance threshold. To examine individual differences in mechanisms of response inhibition, we extracted the medians of all participant-level posterior distributions.

Multivariate relationship between LC integrity and response inhibition. The prediction of response inhibition by LC integrity was tested using a multivariate approach with a two-level procedure (Tsvetanov et al., 2016, 2018, 2021; Passamonti et al., 2019). In the first level, the multidimensional relationship was determined using partial least squares (PLS) (McIntosh and Lobaugh, 2004; Krishnan et al., 2011) with in-house MATLAB scripts. The PLS correlation method is well suited to modest group sizes and situations where the number of variables exceeds the number of participants, as is the case in the current study. PLS described the linear relationship between the two multivariate datasets, namely, all response inhibition parameters and voxelwise LC contrast, based on the singular value decomposition of the cross-covariance matrix between the two datasets. Dataset 1 consisted of all LC voxels across all subjects (62 cases × 274 voxels; LC dataset). Dataset 2 included all response inhibition parameters across all subjects (62 cases × 7 parameters; Response Inhibition dataset). This analysis provided pairs of latent variables ($LV_{inhibition}$ and LV_{LC}) as linear combinations of the original variables that were optimized to maximize their covariance. The same procedure was repeated exclusively in the PD sample (24 cases) to confirm the stability of the obtained latent relationship between voxelwise LC CNRs and response inhibition parameters. All original variables were *z*-scored (mean of 0 and SD of 1) before PLS analysis.

Statistical significance of each pair of latent variables was determined using permutation testing with 10,000 iterations and a significance threshold of $p < 0.05$. Specifically, for each iteration, the rows of the Response Inhibition dataset were randomly reordered, whereas the LC dataset was unaltered, thereby eliminating the participant-wise link between datasets. Null distributions were then obtained by estimating the correlation between latent variables for each iteration of permutation sampling. The *p* value for a given pair of latent variables was computed as the proportion of the null distribution for which the correlation was equal to or greater than the correlation for the original data. The reliability of individual variables contributing to a significant latent variable was assessed by bootstrap ratios (BSRs, 1000 iterations), that is, the weight of the individual variable divided by the bootstrap-estimated SE of that variable (Efron and Tibshirani, 1986). The grouping factor was additionally included to direct the permutation and cross-validation where roughly the same class proportion and equal size as the original group distribution were drawn to avoid biased sampling from the same subgroup. Both loadings of latent variables and BSRs were provided for the level of contribution and the reliability measures for response inhibition parameters and voxelwise LC integrity, respectively.

In the second-level analysis, we confirmed the nature of the group-wise relationship between LC integrity and response inhibition ability, and whether this relationship differs between groups, using linear regression models. The dependent variable was subjects' response inhibition latent variable scores ($LV_{inhibition}$) from the first-level PLS. Predictor variables included subject LC integrity latent variable scores (LV_{LC}) from the first-level PLS, group identity, and their interaction term. Subsequent regression models examined the effects of nuisance covariates, including age, global and local atrophy, disease duration, and motor severity. To mitigate the potential placebo and/or practice effects in the 18 of 24 of the PD patients who completed the task as part of a drug study (O'Callaghan et al., 2021), we adopted two approaches. In a first model, a categorical variable indicated practice (0 = first/only session; 1 = second session); while in a second model, a categorical indicator was added for both practice and placebo effects (0 = one session without placebo; 1 = first session on placebo; 2 = second session on placebo). Adding either of these categorical indicators as a covariate of no interest in the regression models did not meaningfully change the results. Before analysis, continuous variables were *z*-scored, and categorical variables (including nuisance covariates) were assigned sum-to-zero contrasts.

Results

Basic task performance

Participant characteristics and clinical summary data are presented in Table 1. Groups were similar by age, sex, and education,

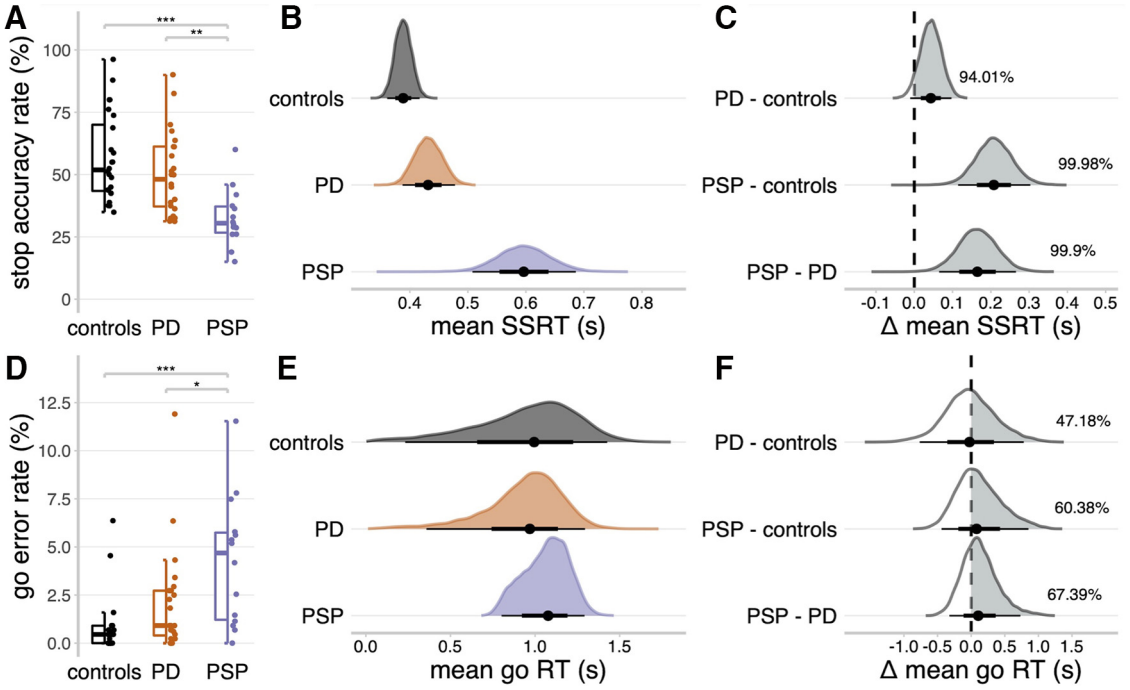

Figure 3. Stop signal task performance. ***A***, ***D***, Proportions of successful stop trials (***A***) and incorrect go responses (***D***). Statistical significance of comparing groups: ***$p < 0.001$; **$p < 0.01$; *$p < 0.005$; *post hoc* Tukey's tests. ***B***, ***E***, Posterior distributions of the mean SSRTs (***B***) and mean go RTs (***E***). Black dots represent the medians. Thick black line segments indicate the 66% QIs. Thin black line segments indicate the 95% QIs. ***C***, ***F***, Posterior distributions of group comparisons for the mean SSRT (***C***) and mean go RT (***F***). Percentages indicate the proportion of the posterior distribution that is strictly positive (i.e., the gray shaded area).

while the patient groups were similar by disease duration and motor severity, although cognitive function was lower in PSP. There were expected significant main effects of group on both the stop accuracy rate (Fig. 3*A*; $F_{(2,59)} = 10.21$, $p < 0.001$; $BF = 143.66$) and go error rate (Fig. 3*D*; $F_{(2,59)} = 8.46$, $p < 0.001$; $BF = 46.85$). *Post hoc* tests indicated that these effects were driven by patients with PSP, who had reduced response accuracy compared with the other groups.

The mean go RT (Fig. 3*E*) was similar across PSP (median = 1.08 s, 95% QI: [0.80, 1.29]), PD (median = 0.97 s, 95% QI: [0.36, 1.30]), and control (median = 1.00 s, 95% QI: [0.23, 1.43]) groups (Fig. 3*F*). However, the mean SSRT was longer in PSP (Fig. 3*B*; median = 0.60 s, 95% QI: [0.51, 0.69]) compared with controls (Fig. 3*C*; median = 0.39 s, 95% QI: [0.36, 0.42]; Δ PSP - controls: median = 0.21 s, 95% QI: [0.11, 0.30], $P_{dir} = 99.98\%$) and PD (median = 0.43 s, 95% QI: [0.39, 0.48]; Δ PSP - PD: median = 0.16 s, 95% QI: [0.06, 0.27], $P_{dir} = 99.90\%$), confirming the expected impairment of response inhibition. The SSRT was also longer in PD compared with controls (Fig. 3*B*; Δ PD – controls: median = 0.04 s, 95% QI: [−0.01, 0.10], $P_{dir} = 94.01\%$).

Processes underlying response inhibition deficits

Following Zhang et al. (2016), the mean threshold height was confirmed as lower in PSP (Fig. 4*A*; median = 2.17, 95% QI: [1.93, 2.40]) relative to controls (Fig. 4*B*; median = 3.31, 95% QI: [2.69, 3.80]; Δ PSP - controls: median = −1.14, 95% QI: [−1.68, −0.49], $P_{dir} = 99.71\%$) and PD (median = 3.02, 95% QI: [2.38, 3.53]; Δ PSP - PD: median = −0.85, 95% QI: [−1.41, −0.18], $P_{dir} = 98.99\%$). The nondecision time was slower in PSP (Fig. 4*C*; median = 0.22 s, 95% QI: [0.11, 0.34]) relative to controls (Fig. 4*D*; median = 0.11 s, 95% QI: [0.10, 0.13]; Δ PSP - controls: median = 0.11 s, 95% QI: [−0.004, 0.23], $P_{dir} = 96.37\%$) and PD (median = 0.12 s, 95% QI: [0.10, 0.16]; Δ PSP - PD: median = 0.10 s, 95% QI: [−0.02, 0.22], $P_{dir} = 93.67\%$). However, the posterior estimate of PSP patients' nondecision time was imprecise (Fig. 4*C*), suggesting that a slower nondecision time was not a feature across all patients with PSP.

We estimated the probabilities of failing to trigger the stop process (trigger failure) and go processes (go failure). The mean probit-transformed trigger failure probability was higher in PSP (Fig. 5*A*; median = −1.78, 95% QI: [−2.68, −0.87]) compared with controls (Fig. 5*B*; median = −3.06, 95% QI: [−3.71, −2.40]; Δ PSP - controls: median = 1.27, 95% QI: [0.18, 2.40], $P_{dir} = 98.85\%$). The mean probit-transformed go failure probability was higher in the PSP group (Fig. 5*C*; median = −2.78, 95% QI: [−3.12, −2.40]) compared with the control (Fig. 5*D*; median = −3.74, 95% QI: [−4.13, −3.35]; Δ PSP - controls: median = 0.96, 95% QI: [0.45, 1.49], $P_{dir} = 99.98\%$) and PD group (median = −3.46, 95% QI: [−3.81, −3.12]; Δ PSP - PD: median = 0.69, 95% QI: [0.21, 1.19], $P_{dir} = 99.76\%$). There were no meaningful differences between the PD and control groups on these attentional parameters (Fig. 5*B*,*D*; all $P_{dir} < 90\%$).

7T MR measurement of LC integrity

Disease-related brain atrophy was not found in medulla ($F_{(2,58)} = 0.48$, $p = 0.62$), pons ($F_{(2,58)} = 2$, $p = 0.14$), or the whole brainstem ($F_{(2,58)} = 2.39$, $p = 0.10$). There was a significant group effect on midbrain volume ($F_{(2,58)} = 5.59$, $p = 0.006$) where the midbrain atrophy was evident in PSP compared with controls ($p_{holm} = 0.008$) and PD ($p_{holm} = 0.01$). LC CNR was not correlated with individual brainstem volumes as examined in linear regression models with total intracranial volume as covariate (medulla: $\beta = 0.11$, $p = 0.15$, pons: $\beta = 0.1$, $p = 0.46$, midbrain: $\beta = 0.15$, $p = 0.24$, whole brainstem: $\beta = 0.12$, $p = 0.36$).

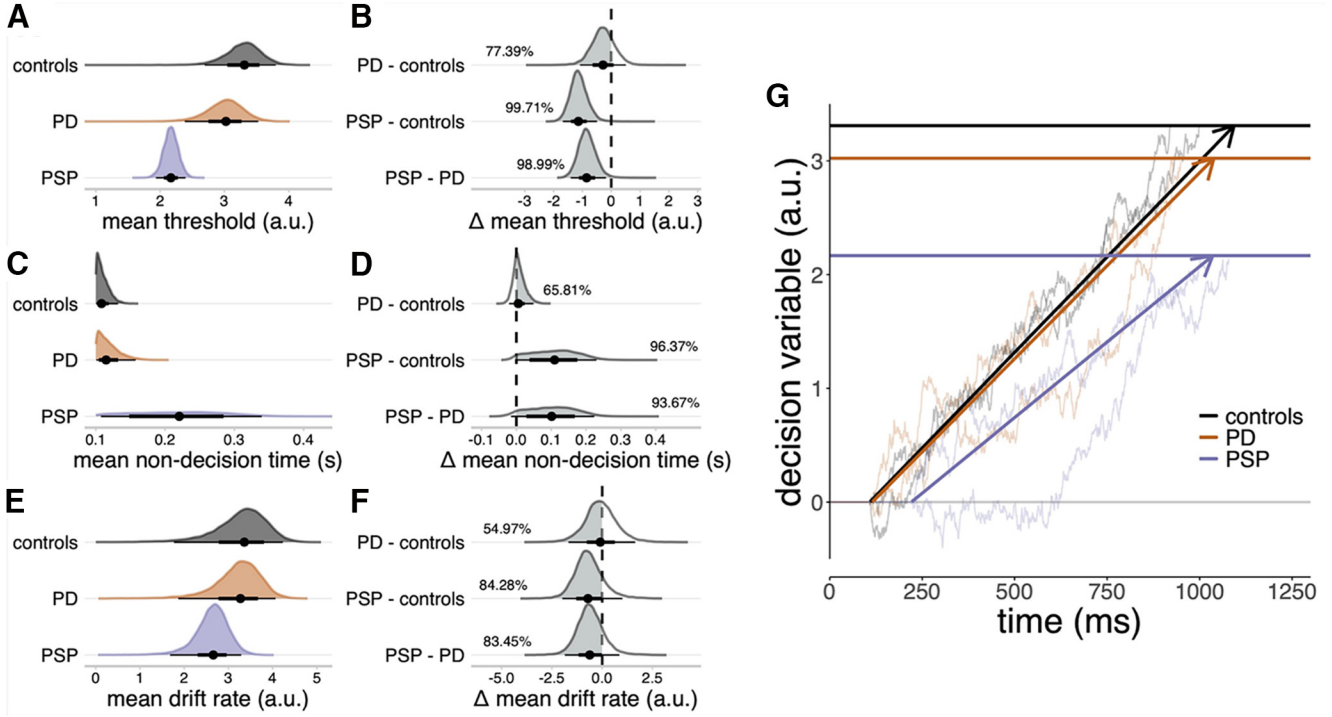

Figure 4. Sequential sampling model of go responses. ***A***, ***C***, ***E***, Posterior distributions of mean threshold (***A***), mean nondecision time (***C***), and mean drift rate (***E***). Black dots represent the medians. Thick black line segments indicate the 66% QIs. Thin black line segments indicate the 95% QIs. ***B***, ***D***, ***E***, Posterior distributions of group comparisons for the mean threshold (***B***), mean nondecision time (***D***), and mean drift rate (***F***). Percentages indicate the proportion of the posterior that is strictly negative (***B***, ***F***) or positive (***D***), that is, the gray shaded area. ***G***, Schematic illustration of the sequential sampling model. Evidence for a go response accumulates stochastically at a constant average rate (the drift rate) until a threshold is reached. To explain RTs, the time taken by the accumulator to reach the threshold is offset by a constant nondecision time. Bold horizontal lines indicate the posterior median estimates of the mean thresholds. Bold directed lines indicate the posterior median estimates of the mean drift rate. Thin lines provide examples of simulated random walks.

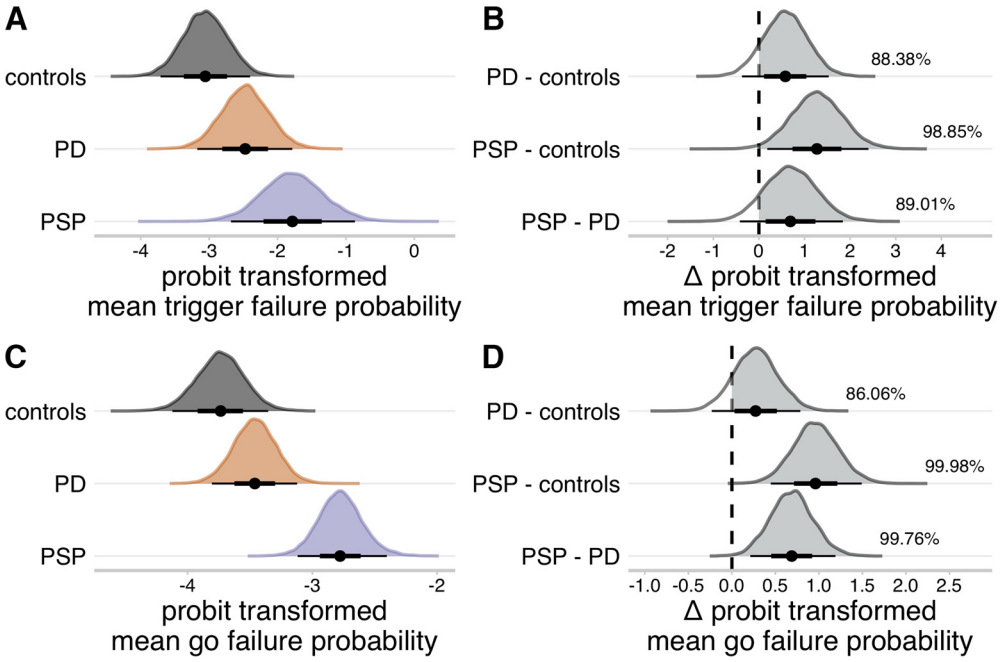

Figure 5. Group-level means of attentional failure parameters. ***A***, ***C***, Posterior distributions of probit transformed mean trigger failure probability (***A***), and probit transformed mean go failure probability (***C***). Black dots represent the medians. Thick black line segments indicate the 66% QIs. Thin black line segments indicate the 95% QIs. ***B***, ***D***, Posterior distributions of group comparisons for the probit transformed mean trigger failure probability (***B***) and probit transformed mean go failure probability (***D***). Percentages indicate the proportion of the posterior that is strictly positive (i.e., the gray shaded area). The probit function was used to project the attentional failure parameters from the probability scale (0, 1) to the real line ($-\infty$, ∞).

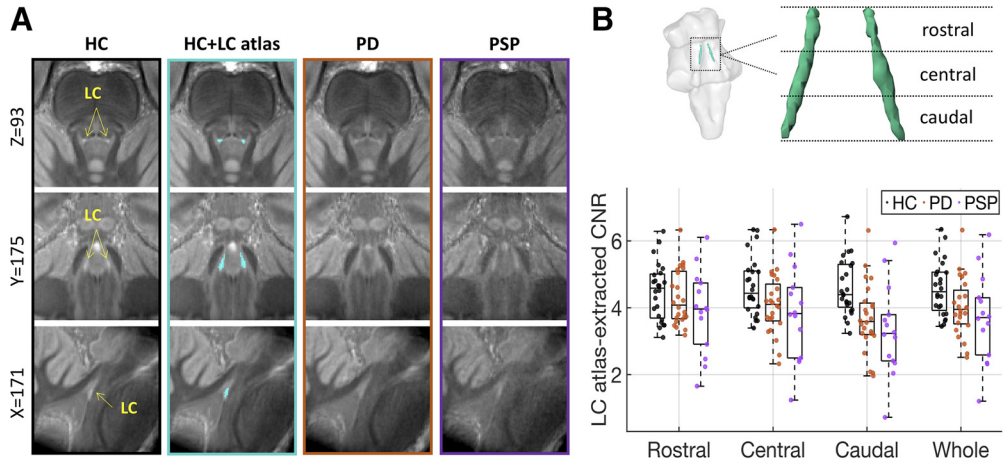

Figure 6. The difference of LC structural integrity in healthy controls and patients. The group averages of the coregistered LC scans were presented (***A***) where PD and PSP patients had diminished contrast in the LC area comparing to the healthy control. The fit of the 25% LC atlas (second column, cyan area) to LC scans was also presented. The averaged contrast to noise ratios of the LC were presented (***B***) for the whole LC and three subregions (rostral, central, and caudal) for individual healthy controls (black dots), PD (orange dots), and PSP patients (purple dots). The group difference was most evident in the caudal LC. Error bars indicate SEs.

Repeated-measures ANOVA revealed a significant effect of LC subregions on the LC signals ($F_{(2118)} = 12.84$, $p < 0.001$), as higher SNR was found in rostral LC compared with central ($p_{holm} < 0.001$) and caudal ($p_{holm} = 0.003$) subregions. The SNR also differed across three groups ($F_{(2,58)} = 4.43$, $p = 0.02$) where higher SNR was seen in the LC area in PD patients comparing with PSP (PD > PSP: $p_{holm} = 0.03$).

The group difference of LC integrity measured with LC CNR was examined using an ANCOVA model by including age, gender, education, midbrain volume, and regional SNR as covariates of no interest. As described in our previous study (R. Ye et al., 2022) and shown in Figure 2*B*, the LC CNR was differed between patients and healthy controls ($F_{(2,54)} = 4.27$, $p = 0.019$) in the caudal subregion where the effect was mainly driven by the difference between patients with PSP and controls ($p_{holm} = 0.025$).

LC integrity and response inhibition

PLS analysis of the response inhibition parameters and voxel-wise LC contrast identified a single significant pair of latent variables ($r = 0.45$, $p = 2.35 \times 10^{-4}$, 10,000 permutations). The LC latent variable (LV_{LC}) expressed negative loadings throughout the structure, to a variable degree across subregions (Fig. 7*A*). Higher scores on this imaging latent variable represent reduced LC integrity. The response inhibition latent variable ($LV_{inhibition}$) expressed positive loadings on the SSRT, go and trigger failure probabilities, and nondecision time, and expressed negative loadings on the drift rate and response threshold of the go process (Fig. 7*C*). Thus, higher scores on this behavioral latent variable reflected impaired response inhibition with prolonged SSRT, greater probability of attentional failures, reduced response threshold, lower drift rate, and longer nondecision time. Mean go RTs had negligible loading on the $LV_{inhibition}$, confirming that a simple summary measure of response execution was not related to the cognitive mechanisms of response inhibition. We also observed a single significant pair of latent variables ($r = 0.53$, $p = 0.008$, 10,000 permutations) with the same pattern of contributions for the LV_{LC} and the $LV_{inhibition}$ by only including the PD patients in the PLS model (Fig. 8*A*,*C*).

The BSRs were also calculated for all response inhibition parameters and for each LC voxel for the identified multivariate relationship. High BSRs > 2 were obtained for SSRT, trigger failure and go failure probabilities, response threshold and nondecision time, indicating that these parameters reliably contributed to the identified $LV_{inhibition}$, whereas lower BSR (i.e., lower reliability, BSR < 2) was found for the drift rate and mean go RT (Fig. 7*D*). For LV_{LC}, all voxels showed high BSRs (>2) where the left caudal LC expressed the highest BSRs comparing to other LC subregions, suggesting that the contribution of left caudal LC was relatively more stable than other LC substructures (Fig. 7*B*). For the BSR results of PD patients, high BSRs were observed for go and trigger failure probabilities among all response inhibition parameters, whereas all LC voxels had BSR > 2, suggesting these measures contributed reliably to the observed latent variables (Fig. 8*B*,*D*).

A regression analysis examined the relationship between response inhibition and LC integrity, and potential group differences. The $LV_{inhibition}$ participant score was the dependent variable, and the LV_{LC} participant score, group, and their interaction were independent variables. In the following analyses and in Figure 7*E*, the sign of the LV_{LC} scores was arbitrarily flipped from negative to positive to enable a more intuitive presentation of results, where higher LV_{LC} scores represent greater LC integrity. There was a significant overall relationship between the LV_{LC} scores and the $LV_{inhibition}$ scores (Fig. 5*D*; $\beta = -0.24$, $F_{(1,56)} = 7.23$, $p = 0.009$; $BF = 6.95$). This suggests that individuals with reduced LC integrity have more severe deficits in response inhibition. There was a significant main effect of group on the $LV_{inhibition}$ scores ($F_{(2,56)} = 29.88$, $p < 0.001$; $BF = 1.98 \times 10^7$), reflecting impaired response inhibition in the PSP group compared with the control group ($t_{(56)} = 7.46$, $p < 0.001$) and PD group ($t_{(56)} = 6.33$, $p < 0.001$), regardless of LC integrity. There was no significant interaction effect between the LV_{LC} scores and group ($F_{(2,56)} = 0.31$, $p = 0.734$; $BF = 0.15$), suggesting that the slope between the LV_{LC} and $LV_{inhibition}$ scores is similar across groups.

We confirmed the robustness of these results with four additional regression analyses. First, adding age, gender, and years of education to the regression model as covariates of no interest did not meaningfully change the relationship between the LV_{LC} and $LV_{inhibition}$ scores ($\beta = -0.23$, $F_{(1,53)} = 6.31$, $p = 0.015$; $BF = 6.99$), nor did the inclusion of additional covariates, including disease duration, motor severity, and local and global brain atrophy. Model selection procedures consistently identified a relatively sparse model as the optimal account of the data, retaining only the LV_{LC} scores and group as predictors of $LV_{inhibition}$

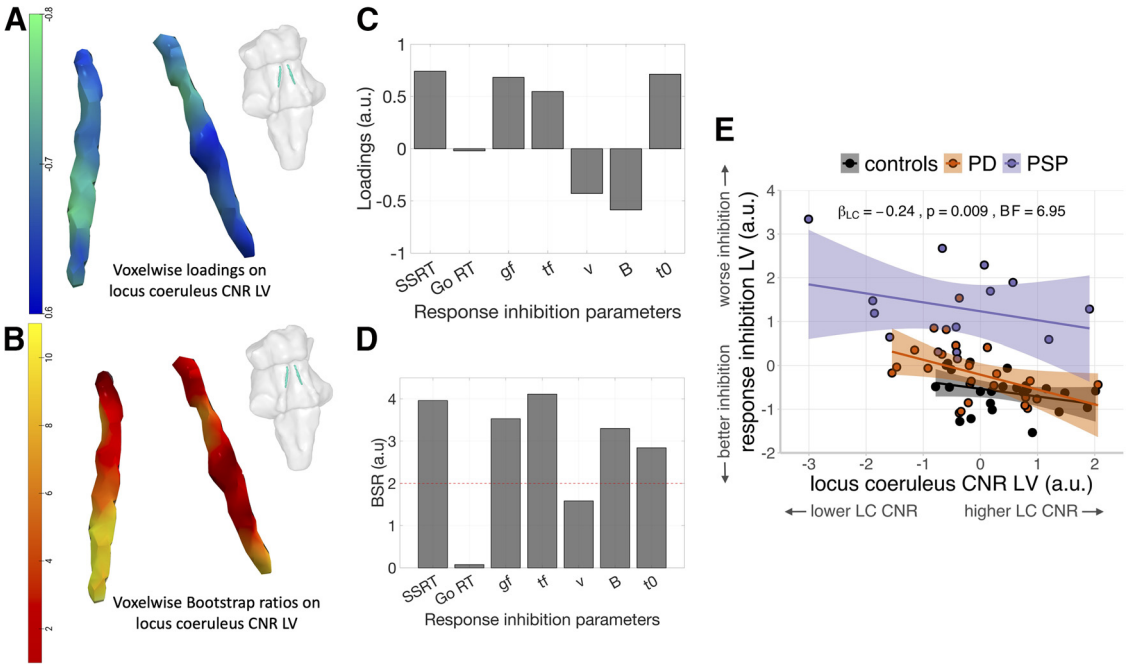

Figure 7. The relationship of LC integrity and response inhibition. As confirmed using PLS, a significant pair of latent variables was identified between voxel-wise LC contrast and response inhibition parameters estimated from cognitive models. ***A***, ***C***, The reliability of the loadings identified in the PLS was assessed using BSRs and was presented for the LC (***B***) and response inhibition parameters (***D***). Negative LC loadings were associated with positive loadings on SSRT, go failure (gf), trigger failure (tf), and nondecision time (t_0), and negative loadings on drift rate (ν) and response threshold (B), whereas loadings on drift rate were less reliable than other parameters as indicated by lower BSR (absolute values < 2). This suggested that impaired response inhibition is linked with reduced LC integrity seen in both PD and PSP patients. An overall relationship of LC integrity and response inhibition was further confirmed in the linear regression model consistent across all groups as supported by a significant main effect of LC when including the group predictor in the model (***E***). Individual fitted lines for each group were presented with curved areas, indicating 95% CIs.

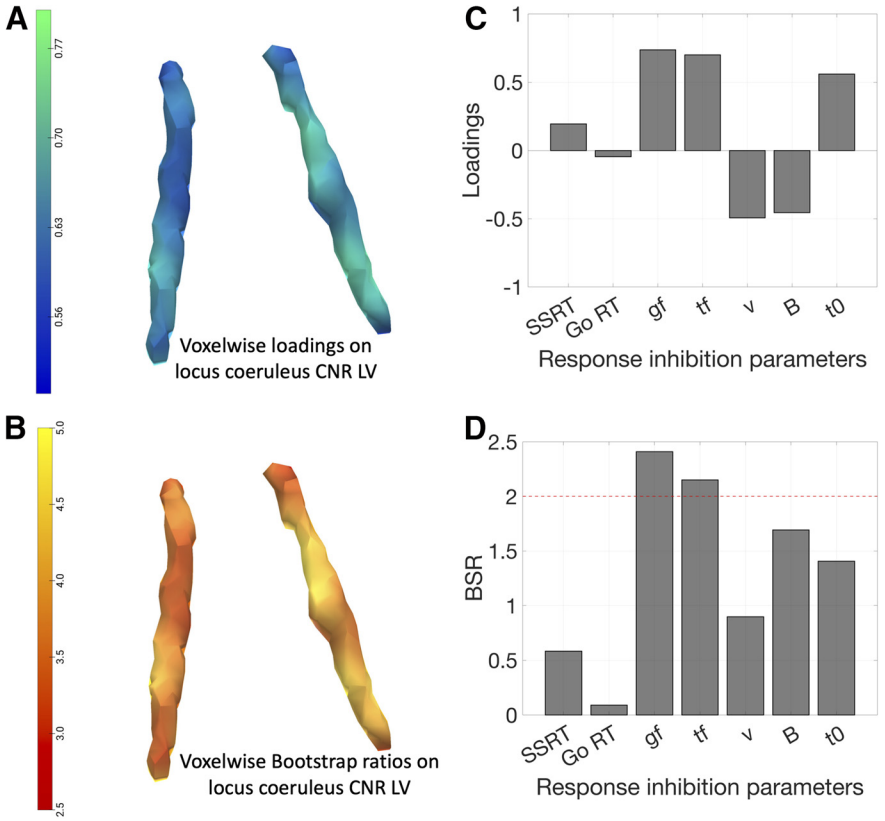

Figure 8. The stability of the latent association between response inhibition and LC integrity. Similar patterns of the latent LC (***A***) and response inhibition (***C***) variables were obtained by testing the PLS model exclusively within PD patients. The BSR assessments (***B***,***D***) for contributing factors in the two latent variables were provided. Reliable factors (BSR > 2) included go and trigger failure probabilities and all LC voxels for the PLS model tested in PD patients.

Table 2. Stepwise selection of predictors of response inhibition scores for the full sample (controls, PD, and PSP groups)[a]

	Model selection step								
Predictors	1	2	3	4	5	6	7	8	$BF_{inclusion}$
LV_{LC}	−0.23*	−0.23*	−0.23*	−0.23*	−0.24**	−0.24**	−0.24**	−0.24**	7.45
Group	−0.76***; −0.41**	−0.75***; −0.40**	−0.73***; −0.39**	−0.75***; −0.39**	−0.77***; −0.40**	−0.73***; −0.38**	−0.69***; −0.35**	−0.68***; −0.35**	7.84×10^6
Gender	0.16	0.18	0.17	0.15	0.14	0.12	0.07	—	0.44
Midbrain	0.41	0.42	0.38	0.41	0.42	0.11	—	—	0.53
Brainstem	−0.27	−0.28	−0.24	−0.27	−0.30	—	—	—	0.46
Education	−0.08	−0.08	−0.07	−0.07	—	—	—	—	0.49
Whole brain	0.06	0.07	0.06	—	—	—	—	—	0.43
Age	−0.06	−0.05	—	—	—	—	—	—	0.41
$LV_{LC} \times$ Group	0.03; −0.07	—	—	—	—	—	—	—	0.23
Information criteria									
AIC	136.68	132.95	131.39	129.85	128.50	127.68	126.98	125.78	
Δ AIC	10.90	7.17	5.62	4.07	2.72	1.90	1.20	0	
BIC	164.33	156.35	152.67	148.99	145.51	142.57	139.74	136.42	
Δ BIC	27.92	19.94	16.25	12.58	9.10	6.15	3.32	0	

[a]Values for predictors under the "Model selection step" columns are standardized regression coefficients (β). $BF_{inclusion}$, Inclusion Bayes factor, that is, the change from before posterior inclusion odds, which indicates how much more likely the data are under models that include the predictor compared with models that exclude the predictor; LV_{LC}, participant scores on latent variable of LC CNR; Group, controls versus PD patients versus PSP patients; Midbrain, total midbrain volume (mm^3); Brainstem, total brainstem volume (mm^3); Whole brain, estimated total intracranial volume (mm^3); AIC, Akaike Information Criterion; BIC, Bayesian Information Criterion; Δ AIC/BIC, difference in AIC/BIC with respect to the lowest AIC/BIC value. The predictors Group and $LV_{LC} \times$ Group are each represented by two regression coefficients: The first coefficient represents the difference between the control group and the intercept; the second coefficient represents the difference between the PD group and the intercept; and the PSP group is modeled as the intercept plus the negative of the sum of the two coefficients.
***$p < 0.001$; **$p < 0.01$; *$p < 0.05$.

(Table 2). Third, rerunning the regression analysis with only the PD and PSP groups yielded a similar relationship between the LV_{LC} and $LV_{inhibition}$ scores ($\beta = -0.26$, $F_{(1,34)} = 4.90$, $p = 0.034$; $BF = 2.07$). Fourth, accounting for potential placebo and/or practice effects in the PD group did not meaningfully change the results. Specifically, the addition of a factor that indicated whether each participant's data were obtained from their first/only testing session versus their second testing session did not meaningfully change the relationship between LV_{LC} and $LV_{inhibition}$ scores ($\beta = -0.24$, $F_{(1,55)} = 7.11$, $p = 0.010$; $BF = 6.86$). Similarly, the addition of a factor that indicated whether each participant's data were obtained from (1) a single session without placebo administration, (2) their first of two sessions, with placebo administration, or (3) their second of two sessions, with placebo administration, did not meaningfully change the relationship between LV_{LC} and $LV_{inhibition}$ scores ($\beta = -0.24$, $F_{(1,54)} = 6.65$, $p = 0.013$; $BF = 6.75$).

Notably, the overall sample size ($N = 62$) was not formally predetermined (e.g., using an *a priori* power analysis). We performed a *post hoc* power analysis using G*Power (version 3.1.9.2) to determine the achieved power for our primary analysis: testing for a linear relationship between the LC latent variable scores (LV_{LC}) and response inhibition latent variable scores ($LV_{inhibition}$), while accounting for group differences and potential interaction effects between group and LV_{LC}. The observed effect size of LV_{LC} ($\beta = -0.24$) within this multiple regression model corresponded to a Cohen's f^2 of 0.13. With a Type I error probability of $\alpha = 0.05$, our sample size of $N = 62$ provides 80% power to detect such an effect ($f^2 = 0.135$) for a single predictor term (here, LV_{LC}), in the context of a multiple linear regression model with five predictors (one predictor for LV_{LC}, two dummy predictors to code for the three groups, and two predictors for interactions between group and LV_{LC}).

Discussion

This study confirms the hypothesis that response inhibition deficits in PD and PSP are linked to structural integrity of the LC, the principal source of cerebral noradrenaline. Diminished response inhibition (i.e., multivariate disinhibition-related parameters) was associated with reduced LC integrity (i.e., multivariate voxelwise loadings) across both groups, in keeping with psychopharmacological and preclinical studies (Bari et al., 2011; Bari and Robbins, 2013; Averbeck et al., 2014; Kehagia et al., 2014; Z. Ye et al., 2015, 2016; Borchert et al., 2016).

The race models identified latent variables to explain the behavioral performance. Despite similar mean RTs in the go responses, there were disease-specific patterns underlying abnormal inhibitory control. Patients with PSP had a reduced response threshold, consistent with a paradoxical bias toward committing go responses as proposed by Zhang et al. (2016), noting that the current study was manual not oculomotor. The PSP group also had a slower nondecision time, suggesting that they required more time for sensory encoding and execution of motor outputs. There was evidence for a lower drift rate among patients with PSP relative to patients with PD and controls, confirming the slower accumulation of evidence to reach a decision.

Task performance might also have been influenced by attentional problems, which are a common cognitive feature in parkinsonian disorders, especially in PSP (Rittman et al., 2013). To account for this possibility, we included attentional failures related to the stop and go processes (i.e., trigger failure and go failure) in the race models of the stop signal task. These indices revealed that patients with PSP had greater attentional deficits than PD and control groups, albeit not to the extent that prevented them from correctly executing the task. The attentional impairments during the stop signal task were also captured within the main PLS-derived $LV_{inhibition}$ variable that related to the LV_{LC} component reflecting LC structural integrity.

The results support the hypothesis that the decision threshold is reduced in PSP to compensate for the impairment in evidence accumulation (reduced drift rate) and execution (slower nondecision time). This threshold compensation is liable to change the quality of decisions, and thereby promote impulsivity. This relationship is disease agnostic and relates to the level of pathology with the LC, which is more severely affected in PSP (R. Ye et al., 2022).

The variability of LC degeneration across patients in our study is also evident postmortem (Cash et al., 1987; Zweig et al., 1993; Kaalund et al., 2020), consistent with what is observed in other neurodegenerative disorders, such as Alzheimer's disease, corticobasal degeneration, and Lewy body dementia (Brunnstrom et al., 2011; Theofilas et al., 2017; Eser et al., 2018; Betts et al., 2019a). This highlights the potential of LC imaging as a transdiagnostic marker to understand individual differences in cognition beyond the classic nosological borders and diagnostic criteria (Betts et al., 2019b).

On average, LC degeneration is more severe in PSP than PD, and our *in vivo* imaging data confirm this, particularly in the caudal portions (Doppler et al., 2021; Madelung et al., 2022; R. Ye et al., 2022). This distribution is consistent with neuropathological studies reporting greater degeneration in the caudal LC (Bertrand et al., 1997). However, the response inhibition deficits spanning PSP and PD topographically map to the mid-caudal and rostral LC (Fig. 7*A*,*B*), that innervate the forebrain regions associated with response inhibition and impulsive behavior (Loughlin et al., 1986).

The LC-noradrenergic system's influence on response inhibition and impulsivity may be nonlinear (e.g., a U-inverted shape function), and involve multiple brain networks (Bari et al., 2011; Cools and D'Esposito, 2011; Bari and Robbins, 2013). The LC diffusely projects to many sites within the brain where noradrenaline has a state-dependent effect on the neuronal input–output gain function (Shine et al., 2021). Although we did not directly measure noradrenaline transmission or noradrenergic receptor density, LC structural integrity is a proxy index of physiological and cognitive functions that are modulated by the LC and impaired in neurodegenerative disorders (Sommerauer et al., 2018; Betts et al., 2019b). The *in vivo* imaged LC integrity reflects the LC cell density as diminished LC contrast is a sign for the loss of pigmented neurons (Sulzer et al., 2018), but it may also relate to the function of the LC-noradrenergic system based on the assumption that presynaptic LC cell loss is accompanied by the impairment of its postsynaptic function. Behavioral and imaging studies have supported this structure–function relationship, with reduced LC integrity being associated with impaired cognitive function and more severe clinical symptoms (Liu et al., 2020; Madelung et al., 2022; Tomassini et al., 2022; R. Ye et al., 2022), although future studies are warranted to determine the underlying neural mechanism and how other factors, such as aging, interacts with the LC structure–function relationship.

Our study focused on noradrenergic contributions to response inhibition deficits in parkinsonian disorders. However, we recognize that noradrenergic projections from the LC have secondary pharmacological interactions with other neurotransmitter systems, including dopamine and GABA. For example, dopamine and noradrenaline can be coreleased from the same LC-noradrenergic terminals (Devoto et al., 2001, 2005a,b). LC activity can alter midbrain dopamine cell firing (Mejias-Aponte, 2016) and directly participate in the regulation of dopamine release in hippocampus (Duszkiewicz et al., 2019). Moreover, there might be a closer link between dopaminergic function and response inhibition deficits (often at a decisional level) in a subset of PD patients with impulse control disorders (Weintraub et al., 2015). Nevertheless, pharmacological studies using selective dopamine manipulations have found no effects on response inhibition (Overtoom et al., 2003; Bari et al., 2009; Obeso et al., 2011a), and there is no clear evidence for a relationship between response inhibition and the levodopa equivalent daily dose or the on/off state of dopaminergic medication in PD (Obeso et al., 2011b; Nombela et al., 2014). Together, our results are consistent with a growing body of work that indicates a robust link between the LC-noradrenaline system and response inhibition, although further work is needed to elucidate the potential contribution of dopaminergic mechanisms. However, we anticipate that any future use of noradrenergic treatments that target response inhibition deficits would be adjunctive to standard dopaminergic therapy, and not an alternative. Therefore, all patients were tested on their usual clinically optimised dopaminergic medication. We acknowledge that patients' task performance may have differed if they were taken off their dopaminergic medication, which consequently could have affected the relationship between response inhibition and LC integrity.

Our study has several limitations. We acknowledge that all the patients were diagnosed with clinical criteria, without pathologic confirmation. Misclassification of PSP subtypes and other atypical parkinsonian syndromes can occur for PSP-Richardson's syndrome diagnosis (Jabbari et al., 2020); and future studies, including postmortem confirmation, would be critical to enhance the diagnostic accuracy. Our study did not include PD patients with impulse control disorders and dementia. However, the impairment of response inhibition is not confined to that minority patients with impulse control disorders; while cognitive impairments are common in nondemented patients. The mechanisms underlying the response inhibition deficits in these phenotypes are likely to include LC-noradrenergic systems that affect other patients, but might involve additional interactions with dopaminergic and cholinergic pathways. Data from some patients with PD were drawn from a placebo-controlled drug study (O'Callaghan et al., 2021). Only the placebo data were analyzed, but we acknowledge that this might have resulted in heterogeneity because of effects of placebo expectancy and/or task practice. To mitigate these issues, we used two approaches to explicitly model the impact of placebo/practice confounds in the statistical analyses. Reassuringly, neither of these steps meaningfully altered the results.

In conclusion, our study elucidates the role of the LC noradrenergic system in response inhibition and its impairment in PD and PSP. Individual differences in response to drug are marked (O'Callaghan et al., 2021) due in part to variation in disease severity, and its impact on brain structure and function, including the integrity of the LC (Ramoz et al., 2009; Whelan et al., 2012; Z. Ye et al., 2014, 2015, 2016; Borchert et al., 2016; O'Callaghan et al., 2021). We propose that LC imaging could be used as a heuristic stratification marker in clinical trials, targeting response inhibition deficits with noradrenergic drugs in those most likely to benefit. Optimization of noradrenergic treatments will benefit from better understanding the mechanisms of response inhibition and their relationship to the integrity of the LC.

References

Averbeck BB, O'Sullivan SS, Djamshidian A (2014) Impulsive and compulsive behaviors in Parkinson's disease. Annu Rev Clin Psychol 10:553–580.

Bari A, Robbins TW (2013) Inhibition and impulsivity: behavioral and neural basis of response control. Prog Neurobiol 108:44–79.

Bari A, Eagle DM, Mar AC, Robinson ES, Robbins TW (2009) Dissociable effects of noradrenaline, dopamine, and serotonin uptake blockade on stop task performance in rats. Psychopharmacology (Berl) 205:273–283.

Bari A, Mar AC, Theobald DE, Elands SA, Oganya KC, Eagle DM, Robbins TW (2011) Prefrontal and monoaminergic contributions to stop-signal task performance in rats. J Neurosci 31:9254–9263.

Bertrand E, Lechowicz W, Szpak GM, Dymecki J (1997) Qualitative and quantitative analysis of locus coeruleus neurons in Parkinson's disease. Folia Neuropathol 35:80–86.

Betts MJ, Cardenas-Blanco A, Kanowski M, Spottke A, Teipel SJ, Kilimann I, Jessen F, Duzel E (2019a) Locus coeruleus MRI contrast is reduced in Alzheimer's disease dementia and correlates with CSF Abeta levels. Alzheimers Dement (Amst) 11:281–285.

Betts MJ, et al. (2019b) Locus coeruleus imaging as a biomarker for noradrenergic dysfunction in neurodegenerative diseases. Brain 142:2558–2571.

Borchert RJ, Rittman T, Passamonti L, Ye Z, Sami S, Jones SP, Nombela C, Vazquez Rodriguez P, Vatansever D, Rae CL, Hughes LE, Robbins TW, Rowe JB (2016) Atomoxetine enhances connectivity of prefrontal networks in Parkinson's disease. Neuropsychopharmacology 41:2171–2177.

Braak H, Del Tredici K, Rub U, de Vos RA, Jansen Steur EN, Braak E (2003) Staging of brain pathology related to sporadic Parkinson's disease. Neurobiol Aging 24:197–211.

Brunnstrom H, Friberg N, Lindberg E, Englund E (2011) Differential degeneration of the locus coeruleus in dementia subtypes. Clin Neuropathol 30:104–110.

Cash R, Dennis T, L'Heureux R, Raisman R, Javoy-Agid F, Scatton B (1987) Parkinson's disease and dementia: norepinephrine and dopamine in locus ceruleus. Neurology 37:42–46.

Chamberlain SR, Del Campo N, Dowson J, Muller U, Clark L, Robbins TW, Sahakian BJ (2007) Atomoxetine improved response inhibition in adults with attention deficit/hyperactivity disorder. Biol Psychiatry 62:977–984.

Chamberlain SR, Hampshire A, Muller U, Rubia K, Del Campo N, Craig K, Regenthal R, Suckling J, Roiser JP, Grant JE, Bullmore ET, Robbins TW, Sahakian BJ (2009) Atomoxetine modulates right inferior frontal activation during inhibitory control: a pharmacological functional magnetic resonance imaging study. Biol Psychiatry 65:550–555.

Chandler DJ, Jensen P, McCall JG, Pickering AE, Schwarz LA, Totah NK (2019) Redefining noradrenergic neuromodulation of behavior: impacts of a modular locus coeruleus architecture. J Neurosci 39:8239–8249.

Clarke WT, Mougin O, Driver ID, Rua C, Morgan AT, Asghar M, Clare S, Francis S, Wise RG, Rodgers CT, Carpenter A, Muir K, Bowtell R (2020) Multi-site harmonization of 7 tesla MRI neuroimaging protocols. Neuroimage 206:116335.

Cools R, D'Esposito M (2011) Inverted-U-shaped dopamine actions on human working memory and cognitive control. Biol Psychiatry 69:e113–e125.

Dalley JW, Robbins TW (2017) Fractionating impulsivity: neuropsychiatric implications. Nat Rev Neurosci 18:158–171.

Dalley JW, Everitt BJ, Robbins TW (2011) Impulsivity, compulsivity, and top-down cognitive control. Neuron 69:680–694.

Del Campo N, Chamberlain SR, Sahakian BJ, Robbins TW (2011) The roles of dopamine and noradrenaline in the pathophysiology and treatment of attention-deficit/hyperactivity disorder. Biol Psychiatry 69:e145–e157.

Devoto P, Flore G, Pani L, Gessa GL (2001) Evidence for co-release of noradrenaline and dopamine from noradrenergic neurons in the cerebral cortex. Mol Psychiatry 6:657–664.

Devoto P, Flore G, Saba P, Fa M, Gessa GL (2005a) Stimulation of the locus coeruleus elicits noradrenaline and dopamine release in the medial prefrontal and parietal cortex. J Neurochem 92:368–374.

Devoto P, Flore G, Saba P, Fa M, Gessa GL (2005b) Co-release of noradrenaline and dopamine in the cerebral cortex elicited by single train and repeated train stimulation of the locus coeruleus. BMC Neurosci 6:31.

Doppler CEJ, Kinnerup MB, Brune C, Farrher E, Betts M, Fedorova TD, Schaldemose JL, Knudsen K, Ismail R, Seger AD, Hansen AK, Staer K, Fink GR, Brooks DJ, Nahimi A, Borghammer P, Sommerauer M (2021) Regional locus coeruleus degeneration is uncoupled from noradrenergic terminal loss in Parkinson's disease. Brain 144:2732–2744.

Duszkiewicz AJ, McNamara CG, Takeuchi T, Genzel L (2019) Novelty and dopaminergic modulation of memory persistence: a tale of two systems. Trends Neurosci 42:102–114.

Efron B, Tibshirani R (1986) Bootstrap methods for standard errors, confidence intervals, and other measures of statistical accuracy. Statistical science 1:54–75.

Erga AH, Alves G, Tysnes OB, Pedersen KF (2020) Impulsive and compulsive behaviors in Parkinson's disease: impact on quality of and satisfaction with life, and caregiver burden. Parkinsonism Relat Disord 78:27–30.

Eser RA, Ehrenberg AJ, Petersen C, Dunlop S, Mejia MB, Suemoto CK, Walsh CM, Rajana H, Oh J, Theofilas P, Seeley WW, Miller BL, Neylan TC, Heinsen H, Grinberg LT (2018) Selective vulnerability of brainstem nuclei in distinct tauopathies: a postmortem study. J Neuropathol Exp Neurol 77:149–161.

Fonov V, Evans AC, Botteron K, Almli CR, McKinstry RC, Collins DL, Brain Development Cooperative Group (2011) Unbiased average age-appropriate atlases for pediatric studies. Neuroimage 54:313–327.

Hauw JJ, Daniel SE, Dickson D, Horoupian DS, Jellinger K, Lantos PL, McKee A, Tabaton M, Litvan I (1994) Preliminary NINDS neuropathologic criteria for Steele-Richardson-Olszewski syndrome (progressive supranuclear palsy). Neurology 44:2015–2019.

Heathcote A, Popiel SJ, Mewhort DJ (1991) Analysis of response time distributions: an example using the Stroop task. Psychol Bull 109:340–347.

Heathcote A, Lin YS, Reynolds A, Strickland L, Gretton M, Matzke D (2019) Dynamic models of choice. Behav Res Methods 51:961–985.

Jabbari E, et al. (2020) Diagnosis across the spectrum of progressive supranuclear palsy and corticobasal syndrome. JAMA Neurol 77:377–387.

Kaalund SS, Passamonti L, Allinson KS, Murley AG, Robbins TW, Spillantini MG, Rowe JB (2020) Locus coeruleus pathology in progressive supranuclear palsy, and its relation to disease severity. Acta Neuropathol Commun 8:11.

Kehagia AA, Housden CR, Regenthal R, Barker RA, Muller U, Rowe J, Sahakian BJ, Robbins TW (2014) Targeting impulsivity in Parkinson's disease using atomoxetine. Brain 137:1986–1997.

Krishnan A, Williams LJ, McIntosh AR, Abdi H (2011) Partial Least Squares (PLS) methods for neuroimaging: a tutorial and review. Neuroimage 56:455–475.

Li Y, Wang C, Wang J, Zhou Y, Ye F, Zhang Y, Cheng X, Huang Z, Liu K, Fei G, Zhong C, Zeng M, Jin L (2019) Mild cognitive impairment in de novo Parkinson's disease: a neuromelanin MRI study in locus coeruleus. Mov Disord 34:884–892.

Liu KY, Kievit RA, Tsvetanov KA, Betts MJ, Duzel E, Rowe JB, Cam-CAN, Howard R, Hämmerer D (2020) Noradrenergic-dependent functions are associated with age-related locus coeruleus signal intensity differences. Nat Commun 11:1712.

Logan GD, Cowan WB, Davis KA (1984) On the ability to inhibit simple and choice reaction time responses: a model and a method. J Exp Psychol Hum Percept Perform 10:276–291.

Loughlin SE, Foote SL, Bloom FE (1986) Efferent projections of nucleus locus coeruleus: topographic organization of cells of origin demonstrated by three-dimensional reconstruction. Neuroscience 18:291–306.

Madelung CF, Meder D, Fuglsang SA, Marques MM, Boer VO, Madsen KH, Petersen ET, Hejl AM, Lokkegaard A, Siebner HR (2022) Locus coeruleus shows a spatial pattern of structural disintegration in Parkinson's disease. Mov Disord 37:479–489.

Makowski D, Ben-Shachar MS, Chen SH, Ludecke D (2019) Indices of effect existence and significance in the Bayesian framework. Front Psychol 10:2767.

Mason ST, Fibiger HC (1979) Regional topography within noradrenergic locus coeruleus as revealed by retrograde transport of horseradish peroxidase. J Comp Neurol 187:703–724.

Matzke D, Curley S, Gong CQ, Heathcote A (2019) Inhibiting responses to difficult choices. J Exp Psychol Gen 148:124–142.

Matzke D, Logan GD, Heathcote A (2020) A cautionary note on evidence-accumulation models of response inhibition in the stop-signal paradigm. Comput Brain Behav 3:269–288.

McIntosh AR, Lobaugh NJ (2004) Partial least squares analysis of neuroimaging data: applications and advances. Neuroimage 23:S250–S263.

Mejias-Aponte CA (2016) Specificity and impact of adrenergic projections to the midbrain dopamine system. Brain Res 1641:258–273.

Murley AG, Rouse MA, Jones PS, Ye R, Hezemans FH, O'Callaghan C, Frangou P, Kourtzi Z, Rua C, Carpenter TA, Rodgers CT, Rowe JB (2020) GABA and glutamate deficits from frontotemporal lobar degeneration are associated with disinhibition. Brain 143:3449–3462.

Murley AG, Rouse MA, Coyle-Gilchrist IT, Jones PS, Li W, Wiggins J, Lansdall C, Vazquez Rodriguez P, Wilcox A, Patterson K, Rowe JB (2021) Predicting loss of independence and mortality in frontotemporal lobar degeneration syndromes. J Neurol Neurosurg Psychiatry 92:737–744.

Nombela C, Rittman T, Robbins TW, Rowe JB (2014) Multiple modes of impulsivity in Parkinson's disease. PLoS One 9:e85747.

O'Callaghan C, Hezemans FH, Ye R, Rua C, Jones PS, Murley AG, Holland N, Regenthal R, Tsvetanov KA, Wolpe N, Barker RA, Williams-Gray CH, Robbins TW, Passamonti L, Rowe JB (2021) Locus coeruleus integrity

and the effect of atomoxetine on response inhibition in Parkinson's disease. Brain 144:2513–2526.
Obeso I, Wilkinson L, Jahanshahi M (2011a) Levodopa medication does not influence motor inhibition or conflict resolution in a conditional stop-signal task in Parkinson's disease. Exp Brain Res 213:435–445.
Obeso I, Wilkinson L, Casabona E, Bringas ML, Alvarez M, Alvarez L, Pavon N, Rodriguez-Oroz MC, Macias R, Obeso JA, Jahanshahi M (2011b) Deficits in inhibitory control and conflict resolution on cognitive and motor tasks in Parkinson's disease. Exp Brain Res 212:371–384.
Overtoom CC, Verbaten MN, Kemner C, Kenemans JL, van Engeland H, Buitelaar JK, van der Molen MW, van der Gugten J, Westenberg H, Maes RA, Koelega HS (2003) Effects of methylphenidate, desipramine, and L-dopa on attention and inhibition in children with Attention Deficit Hyperactivity Disorder. Behav Brain Res 145:7–15.
Passamonti L, Tsvetanov KA, Jones PS, Bevan-Jones WR, Arnold R, Borchert RJ, Mak E, Su L, O'Brien JT, Rowe JB (2019) Neuroinflammation and Functional Connectivity in Alzheimer's Disease: Interactive Influences on Cognitive Performance. J Neurosci 39:7218–7226.
Ramoz N, Boni C, Downing AM, Close SL, Peters SL, Prokop AM, Allen AJ, Hamon M, Purper-Ouakil D, Gorwood P (2009) A haplotype of the norepinephrine transporter (Net) gene Slc6a2 is associated with clinical response to atomoxetine in attention-deficit hyperactivity disorder (ADHD). Neuropsychopharmacology 34:2135–2142.
Rittman T, Ghosh BC, McColgan P, Breen DP, Evans J, Williams-Gray CH, Barker RA, Rowe JB (2013) The Addenbrooke's Cognitive Examination for the differential diagnosis and longitudinal assessment of patients with parkinsonian disorders. J Neurol Neurosurg Psychiatry 84:544–551.
Robinson ES, Eagle DM, Mar AC, Bari A, Banerjee G, Jiang X, Dalley JW, Robbins TW (2008) Similar effects of the selective noradrenaline reuptake inhibitor atomoxetine on three distinct forms of impulsivity in the rat. Neuropsychopharmacology 33:1028–1037.
Ryu DW, Kim JS, Yoo SW, Oh YS, Lee KS (2019) The impact of impulsivity on quality of life in early drug-naive Parkinson's disease patients. J Mov Disord 12:172–176.
Sara SJ (2009) The locus coeruleus and noradrenergic modulation of cognition. Nat Rev Neurosci 10:211–223.
Shine JM, Muller EJ, Munn B, Cabral J, Moran RJ, Breakspear M (2021) Computational models link cellular mechanisms of neuromodulation to large-scale neural dynamics. Nat Neurosci 24:1046.
Sommerauer M, Fedorova TD, Hansen AK, Knudsen K, Otto M, Jeppesen J, Frederiksen Y, Blicher JU, Geday J, Nahimi A, Damholdt MF, Brooks DJ, Borghammer P (2018) Evaluation of the noradrenergic system in Parkinson's disease: an 11C-MeNER PET and neuromelanin MRI study. Brain 141:496–504.
Sulzer D, Cassidy C, Horga G, Kang UJ, Fahn S, Casella L, Pezzoli G, Langley J, Hu XP, Zucca FA, Isaias IU, Zecca L (2018) Neuromelanin detection by magnetic resonance imaging (MRI) and its promise as a biomarker for Parkinson's disease. NPJ Parkinsons Dis 4:11.
Theofilas P, Ehrenberg AJ, Dunlop S, Di Lorenzo Alho AT, Nguy A, Leite RE, Rodriguez RD, Mejia MB, Suemoto CK, Ferretti-Rebustini RE, Polichiso L, Nascimento CF, Seeley WW, Nitrini R, Pasqualucci CA, Filho WJ, Rueb U, Neuhaus J, Heinsen H, Grinberg LT (2017) Locus coeruleus volume and cell population changes during Alzheimer's disease progression: a stereological study in human postmortem brains with potential implication for early-stage biomarker discovery. Alzheimers Dement 13:236–246.
Tomassini A, Hezemans FH, Ye R, Tsvetanov KA, Wolpe N, Rowe JB (2022) Prefrontal cortical connectivity mediates locus coeruleus noradrenergic regulation of inhibitory control in older adults. J Neurosci 42:3484–3493.
Tsvetanov KA, Henson RN, Tyler LK, Razi A, Geerligs L, Ham TE, Rowe JB, Cambridge Centre for A, Neuroscience (2016) Extrinsic and Intrinsic Brain Network Connectivity Maintains Cognition across the Lifespan Despite Accelerated Decay of Regional Brain Activation. J Neurosci 36:3115–3126.
Tsvetanov KA, Ye Z, Hughes L, Samu D, Treder MS, Wolpe N, Tyler LK, Rowe JB, Cambridge Centre for A, Neuroscience (2018) Activity and Connectivity Differences Underlying Inhibitory Control Across the Adult Life Span. J Neurosci 38:7887–7900.
Tsvetanov KA, et al. (2021) Brain functional network integrity sustains cognitive function despite atrophy in presymptomatic genetic frontotemporal dementia. Alzheimers Dement 17:500–514.
Wang J, Li Y, Huang Z, Wan W, Zhang Y, Wang C, Cheng X, Ye F, Liu K, Fei G, Zeng M, Jin L (2018) Neuromelanin-sensitive magnetic resonance imaging features of the substantia nigra and locus coeruleus in de novo Parkinson's disease and its phenotypes. Eur J Neurol 25:949–973.
Weintraub D, David AS, Evans AH, Grant JE, Stacy M (2015) Clinical spectrum of impulse control disorders in Parkinson's disease. Mov Disord 30:121–127.
Whelan R, et al., IMAGEN Consortium (2012) Adolescent impulsivity phenotypes characterized by distinct brain networks. Nat Neurosci 15:920–925.
Ye R, Rua C, O'Callaghan C, Jones PS, Hezemans FH, Kaalund SS, Tsvetanov KA, Rodgers CT, Williams G, Passamonti L, Rowe JB (2021) An in vivo probabilistic atlas of the human locus coeruleus at ultra-high field. Neuroimage 225:117487.
Ye R, O'Callaghan C, Rua C, Hezemans FH, Holland N, Malpetti M, Jones PS, Barker RA, Williams-Gray CH, Robbins TW, Passamonti L, Rowe J (2022) Locus coeruleus integrity from 7 T MRI relates to apathy and cognition in Parkinsonian disorders. Mov Disord 37:1663–1672.
Ye Z, Altena E, Nombela C, Housden CR, Maxwell H, Rittman T, Huddleston C, Rae CL, Regenthal R, Sahakian BJ, Barker RA, Robbins TW, Rowe JB (2014) Selective serotonin reuptake inhibition modulates response inhibition in Parkinson's disease. Brain 137:1145–1155.
Ye Z, Altena E, Nombela C, Housden CR, Maxwell H, Rittman T, Huddleston C, Rae CL, Regenthal R, Sahakian BJ, Barker RA, Robbins TW, Rowe JB (2015) Improving response inhibition in Parkinson's disease with atomoxetine. Biol Psychiatry 77:740–748.
Ye Z, Rae CL, Nombela C, Ham T, Rittman T, Jones PS, Rodriguez PV, Coyle-Gilchrist I, Regenthal R, Altena E, Housden CR, Maxwell H, Sahakian BJ, Barker RA, Robbins TW, Rowe JB (2016) Predicting beneficial effects of atomoxetine and citalopram on response inhibition in Parkinson's disease with clinical and neuroimaging measures. Hum Brain Mapp 37:1026–1037.
Zhang J, Rittman T, Nombela C, Fois A, Coyle-Gilchrist I, Barker RA, Hughes LE, Rowe JB (2016) Different decision deficits impair response inhibition in progressive supranuclear palsy and Parkinson's disease. Brain 139:161–173.
Zweig RM, Cardillo JE, Cohen M, Giere S, Hedreen JC (1993) The locus ceruleus and dementia in Parkinson's disease. Neurology 43:986–991.